Synthesis of Barium Sulfate Nanoparticles and Nanofilaments in Reverse Micelles and Microemulsions

Jeremy D. Hopwood and Stephen Mann*

School of Chemistry, University of Bath, Bath, BA2 7AY, U.K.

Received February 25, 1997. Revised Manuscript Received June 9, 1997[⊗]

Supersaturated reverse micelles and microemulsions containing either AOT (sodium bis-(2-ethylhexylsulfosuccinate)), $C_{12}EO_4$ (poly(oxyethylene-4-dodecyl ether)), or DDAB (didodecyldimethylammonium bromide) surfactants have been used as organized reaction microenvironments for barium sulfate precipitation. Nanoclusters of amorphous barium sulfate, 2−4 nm in size, were formed in association with BaNaAOT reverse micelles. In contrast, highly elongated filaments of crystalline barium sulfate, with lengths up to 100 μm and aspect ratios of 1000, were formed in BaNaAOT microemulsions. The individual filaments were single crystals of barite elongated predominantly along the [010] axis and in some instances consisted of coaligned nanofilaments, 20−50 nm in width. Similar reactions in $C_{12}EO_4$ reverse micelles and microemulsions afforded barite nanocrystals, 5−7 nm in dimension and tabular-shaped barite crystals, up to 400 nm in size, respectively. Rhombic crystals of barite, approximatety 200 nm in size, were deposited in DDAB microemulsions. No barite filaments were observed in the $C_{12}EO_4$ and DDAB systems. A generalized mechanism for the growth of barite nanofilaments in AOT microemulsions, involving the irreversible fusion, unidirectional exchange, and coalescence of microemulsion droplets, followed by crystallization of an amorphous filamentous $BaSO_4$/surfactant phase, is described.

Introduction

The synthesis of complex inorganic materials with dimensional, structural, and morphological specificity is important for many areas of materials chemistry. Two distinct themes—"template-directed" synthesis and "morphosynthesis"—are currently being investigated.[1] In the former, supramolecular assemblies of organic molecules are exploited as chemically and spatially specific interfaces for the site-directed nucleation, growth, and patterning of inorganic materials. This synthesis approach has been particularly successful in generating a new class of ordered silica and transition-metal oxide mesophases,[2,3] high-axial-ratio inorganic oxides,[4,5] layered inorganic−organic hybrids,[6] and oriented inorganic crystals.[7] Typically, surfactants and lipids have been used in the form of monolayers,[7] cylindrical micelles,[2,3] rod-shaped[4] and helical[5,8] microstructures, and liquid crystals.[9,10]

In the second approach, organized reaction media are employed to constrain and pattern the deposition of spatially confined inorganic precursors. The use of multiphase systems containing restricted aqueous/hydrophilic reaction environments has resulted in a wide range of size-quantized dispersed inorganic nanoparticles. For example, metallic,[11] semiconductor,[12−15] calcium carbonate,[16−18] silica,[19,20] barium sulfate,[21] and zeolite[22,23] nanoparticles have been prepared in reverse micelles and microemulsions. Similarly, lipid vesicles[24−27] and the polypeptide vesicle of the protein, ferritin,[28−31] have been used as confined reaction cavities for the controlled synthesis of dispersed inorganic nanocomposites with magnetic and semiconducting properties.

* Author for correspondence.

[⊗] Abstract published in *Advance ACS Abstracts,* August 1, 1997.

(1) . Mann, S.; Ozin, G. A. *Nature* **1996**, *382*, 313.
(2) Kresge C. T.; Leonowicz M. E.; Roth W. J.; Vartuli J. C.; Beck J. S. *Nature* **1992,** *359*, 710.
(3) Monnier A.; et al. *Science* **1993,** *261*, 1299.
(4) Archibald, D. D.; Mann, S. *Nature* **1993,** *364*, 430.
(5) Baral, S.; Schoen, P. *Chem. Mater.* **1993**, *5*, 145.
(6) Cao, G.; Hong, H.-G.; Mallouk, T. E. *Acc. Chem. Res* **1992**, *25*, 532.
(7) Heywood, B.; R. Mann, S. *Adv. Mater.* **1994,** *6*, 9.
(8) Burkett, S. L.; Mann, S. *Chem. Commun.* **1996**, 321.
(9) Attard, G. S.; Glyde, J. C.; Goltner, C. G. *Nature* **1995**, *378*, 366.
(10) Braun, P. V.; Osenar, P.; Stupp, S. I. *Nature* **1996**, *380*, 325.
(11) Kishida, M.; Fujita, T.; Umakoshi, K.; Ishiyama, J.; Nagata, H.; Wakabayashi, K. *Chem. Commun.* **1995**, 763.
(12) Pileni, M. P.; Motte, L.; Petit, C. *Chem. Mater.* **1992**, *4*, 338.
(13) Kortan, A. R.; Hull, R.; Opila, R. L.; Bawendi, M. G.; Steigerwald, M. L.; Carroll, P. J.; Brus, L. E. *J. Am. Chem. Soc.* **1990**, *112*, 1327.
(14) Petit, C.; Pileni, M. P. *J. Phys Chem.* **1988**, *92*, 2282.
(15) Lianos, P.; Thomas, J. K. *Chem. Phys. Lett.* **1986**, *125*, 299.
(16) Kandori, K.; Kon-No, K.; Kitahara, A. *J. Colloid Interface Sci.* **1987**, *122*, 78.
(17) Kandori, K.; Kon-No, K.; Kitahara, A. *J. Colloid Interface Sci.* **1987**, *115*, 579.
(18) Roman, J, P.; Hoornaert, P.; Faure, D.; Biver, C.; Jacquet, F.; Martin, J, M.; *J. Colloid Interface Sci.* **1990**, *144*, 324.
(19) Arriagada, F. J.; Osseo-Asare, K. *Colloids Surf.* **1992**, *69*, 105.
(20) Arriagada, F. J.; Osseo-Asare, K. *J. Colloid Interface Sci.* **1995**, *170*, 8.
(21) Qi, L.; Ma, J.; Cheng, H.; Zhao, Z. *Colloids Surf. A* **1996** *108*, 117.
(22) Dutta, P. K.; Robins. D. *Langmuir* **1991**, *7*, 1048.
(23) Jakupca, M.; Reddy, S. N.; Salvati, L Dutta, P. K. *Nature* **1995**, *374*, 44.
(24) Nagy, B.; Bodart-Ravet, I.; Derouane, E. G. *Faraday Discuss. Chem. Soc.* **1989**, *87*, 189−198.
(25) Horvath, O.; Fendler, J. H. *J. Phys. Chem.* **1992**, *96*, 9591−9594.
(26) Mann, S.; Hannington, J. P.; Williams, R. J. P. *Nature* **1986**, *324*, 565−567.
(27) Bhandarkar, S.; Bose, A. *J. Colloid. Interface Sci.* **1990**, *135*, 531−538.
(28) Meldrum, F. C.; Wade, V. J.; Nimmo, D. L.; Heywood, B. R.; Mann, S. *Nature* **1991**, *349*, 684.
(29) Meldrum, F. C.; Heywood, B. R.; Mann, S. *Science* **1992**, *257*, 522.
(30) Mackle, P.; Charnock, J. M.; Garner, C. D.; Meldrum, F. C.; Mann, S. *J. Am. Chem. Soc.* **1993**, *115*, 8471.
(31) Douglas, T.; Dickson, D. P. E.; Betteridge, S.; Charnock, J.; Garner, C. D.; Mann, S. *Science* **1995**, *269*, 54.

S0897-4756(97)00113-0 CCC: $14.00 © 1997 American Chemical Society

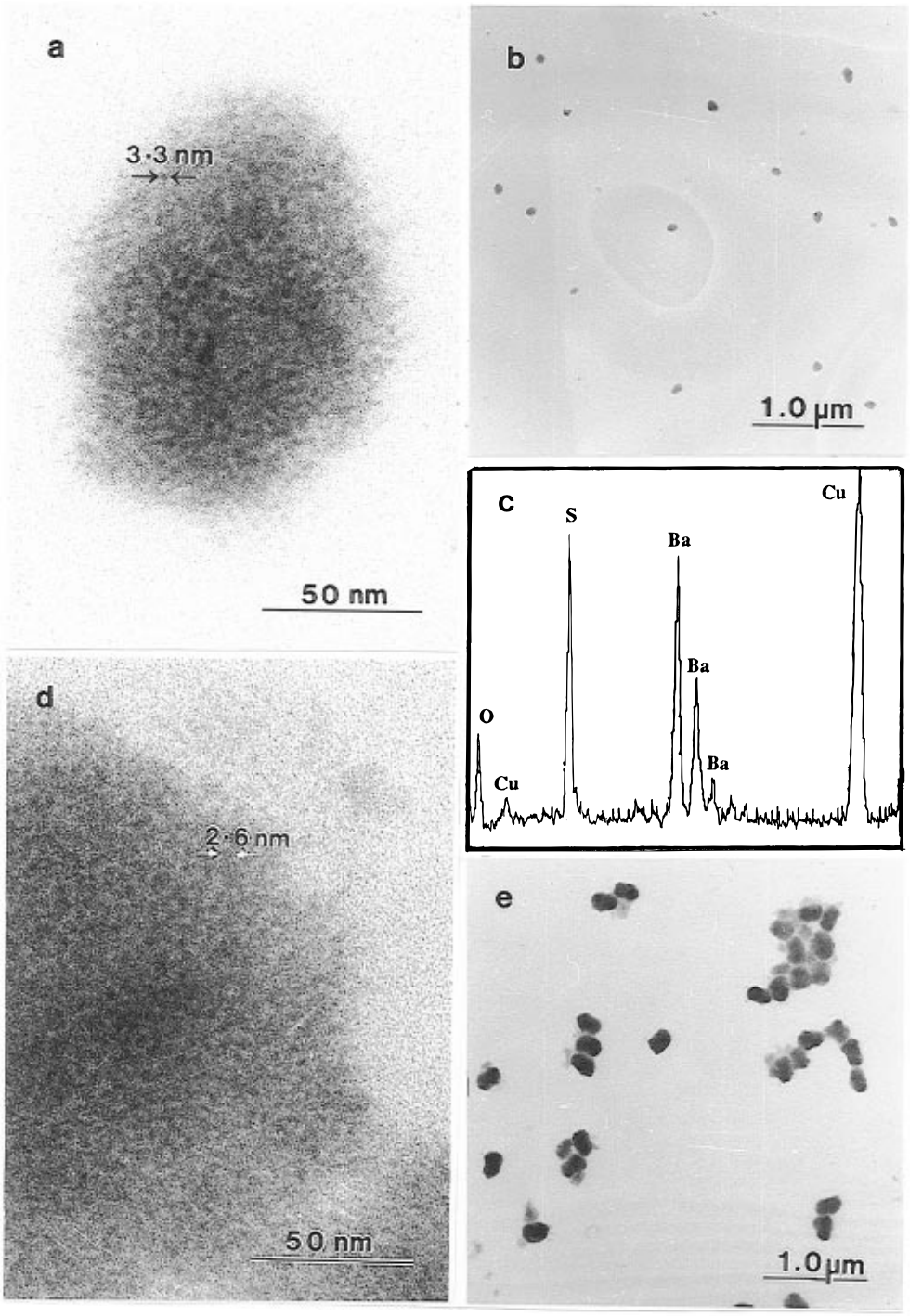

Figure 1. Barium sulfate formation in supersaturated $Ba_{0.019}Na_{0.962}$AOT/isooctane/H_2O reverse micelles, $w = 5$, $S > 800$. (a and b) High and low magnification TEM images, respectively, at [AOT] = 0.1 M. The individual oval-shaped $BaSO_4$ deposit shown in (a) is composed of aggregated amorphous nanoparticles, approximately 3 nm in size. (c) EDXA spectrum recorded from an individual oval-shaped aggregate. (d and e) High and low magnification TEM images, respectively, at [AOT] = 1.46 M. The higher surfactant concentration results in particles larger than those observed at 0.1 M. As shown in (d), individual particles consist of aggregated nanoparticles of amorphous $BaSO_4$/surfactant clusters.

In addition, block copolymers containing hydrophobic and hydrophilic domains have been used to produce ordered arrays of gold nanoparticles.[32]

The above examples of materials synthesis in organized reaction fields highlight the wide range of possibilities offered by multiphase systems for constraining the dimensionality of monodispersed inorganic colloids. However, these systems usually have negligible influence on the shape of the confined inorganic particles. Recently, it has been shown that complex microskeletal inorganic materials can be synthesized within bicontinuous microemulsions prepared from aqueous supersaturated solutions of calcium phosphate or calcium carbonate, didodecyldimethylammonium bromide (DDAB), and long-chain alkane oils with melting points above 0 °C. Because both the calcium phosphate frameworks[33,34] and cellular calcium carbonate thin films[35] are ordered at the micron scale, they are not

(32) Spatz, J. P.; Roescher, A.; Möller, M. *Adv. Mater.* **1996,** *8,* 337.

direct replicas of the bicontinuous microstructure that exhibits order at the nanometer level. These results suggest that complex inorganic forms can be produced by mineralization of transitory microstructures generated within the bicontinuous DDAB-containing microemulsions by localized reorganization and microphase separation.

There are few reports concerning the evolution of shaped inorganic materials synthesized in non-DDAB microemulsion phases. Recently, a report described the formation of highly elongated rods of copper from a liquid-crystalline $CuAOT_2$ lamellar phase.[36] In this paper we describe the deposition of barium sulfate in supersaturated reverse micelles and microemulsions containing either AOT (sodium bis(2-ethylhexylsulfosuccinate)) or $C_{12}EO_4$ (poly(oxyethylene-4-dodecyl ether)) surfactants, and in supersaturated DDAB (didodecyldimethylammonium bromide) microemulsions. We show that crystallization is restricted in BaNaAOT reverse micelles such that amorphous barium sulfate/surfactant nanoclusters are formed. In contrast, unusual high aspect ratio filaments of crystalline barium sulfate (barite) are observed when the synthesis is undertaken in BaNaAOT microemulsions. To our knowledge, this is the first report to describe either the formation of amorphous barium sulfate or synthesis of filamentous barite by microemulsion-mediated reactions. We show that barium sulfate formation in $C_{12}EO_4$ reverse micelles and microemulsions results in crystalline nanoparticles and tabular particles, respectively. Similarly shaped tabular crystals were observed from supersaturated DDAB microemulsions. The results indicate that, under the experimental conditions investigated, the complex filamentous barite morphology is specific to the AOT microemulsion system.

Materials

All materials were of analytical grade (purity ≥98%) and used without further purification. Surfactants were purchased from Aldrich Chemical Co. Sodium AOT (M.W. = 444.55), also known as aerosol OT, sodium bis(2-ethylhexylsulfosuccinate) or as sodium dioctyl sulfosuccinate was a white pastelike solid. Poly(oxyethylene-4-dodecyl ether) ($C_{12}EO_4$, MW = 362.56, density = 0.95 g cm^{-3}) was the commercial product Brij30 and at room temperature was a semiviscous liquid. Didodecyldimethylammonium bromide (DDAB, MW = 462.65) was a powder. All the surfactants were hygroscopic and stored under vacuum. The alkane oils, decane (MW = 142.29, density = 0.73 g cm^{-3}) and dodecane (MW = 170.34, density = 0.75 g cm^{-3}) were purchased from Aldrich. HPLC-grade isooctane also known as 2,2,4-trimethylpentane (MW = 114.23, density = 0.692 g cm^{-3}) was purchased from Fisons Chemicals. Water was double distilled and passed through an organic filtration column.

Sodium AOT was converted to barium AOT (MW = 980.47) by direct precipitation in water with barium chloride. A 0.01% w/w aqueous solution of sodium AOT (0.0225 M) was prepared, and this was mixed with an equal volume of barium chloride solution (0.027 M). The barium AOT product (a white precipitate) was centrifuged, washed with water and then dried under vacuum. The surfactant was then dissolved in isooctane (at a weight ratio of 1:6, respectively), filtered through a 0.22 μm solvent-resistant membrane, and dried for storage using a rotary evaporator and high vacuum. Characterization by flame emission and elemental analysis showed the surfactant to be pure barium AOT and to contain <1% water.

Figure 2. TEM image of a $BaSO_4$ fiber synthesized in a supersaturated (S > 500) $Ba_{0.019}Na_{0.962}AOT$/isooctane/H_2O microemulsion, w = 10, [AOT] = 0.1 M. Multiple filaments of the inorganic mineral can be seen emerging from the end of the fiber.

The extent of the reverse micelle and microemulsion region in the surfactant−water−oil systems of NaAOT, $C_{12}EO_4$, and DDAB was checked against published data[37−40] by measuring the amount of water required to induce phase separation. This was done by slowly adding distilled water dropwise to the surfactant in oil mixtures and recording the maximum amount solubilized.

Methods

Barium Sulfate Formation in BaNaAOT Reverse Micelles and Microemulsions. Supersaturated $Ba_{0.019}Na_{0.962}$-AOT reverse micelles with a surfactant to oil concentration of 0.1 M and [H_2O]/[surfactant] molar ratio w = 5 were prepared by adding an anhydrous solution of $BaAOT_2$ dissolved in isooctane (0.05 M, 1 g, w < 1) to a NaAOT/isooctane/water reverse micelle solution ([surfactant] = 0.1 mol dm^{-3} (isooctane), w = 5, 25 g) containing aqueous Na_2SO_4 (0.02 M). The resulting dispersion was stored at 25 °C, and samples were taken after 24 h and 1 week. This method was repeated at high concentration using an isooctane solution of $BaAOT_2$ (0.18 mol dm^{-3} oil, 1 g) and a NaAOT reverse micelle solution (1.67 mol of surfactant dm^{-3} oil, 9.8 g, w = 5) to produce supersaturated $Ba_{0.019}Na_{0.962}AOT$ reverse micelles with a surfactant to oil concentration of 1.46 M and [H_2O]/[surfactant] molar ratio of 5.

(33) Walsh, D.; Hopwood, J. D.; Mann, S. *Science* **1994**, *264*, 1576.
(34) Walsh, D.; Mann, S. *Chem. Mater.* **1996**, *8*, 1944.
(35) Walsh, D.; Mann, S. *Nature*, **1995,** *377*, 320.
(36) Pileni, M. P.; Tanori, J. *Adv. Mater.* **1995**, *7*, 862.
(37) Skurtveit, R.; Sjoblom, J.; Bouwstra, J.; Gooris, G.; Selle, M.H. *J. Colloid Interface Sci.* **1992**, *152*, 205.
(38) Chen, S. J.; Evans, D. F.; Ninham, B. W.; Mitchell, D. J.; Blum, F. D.; Pickup, S. *J. Phys. Chem.* **1986**, *90*, 842.
(39) Chen, V.; Warr, G. G.; Evans, D. F.; Predergast, F. G. *J. Phys. Chem.* **1988,** *92*, 768.
(40) Chen, V.; Evans, D. F.; Ninham, B. W. *J. Phys. Chem.* **1987,** *91*, 1823.

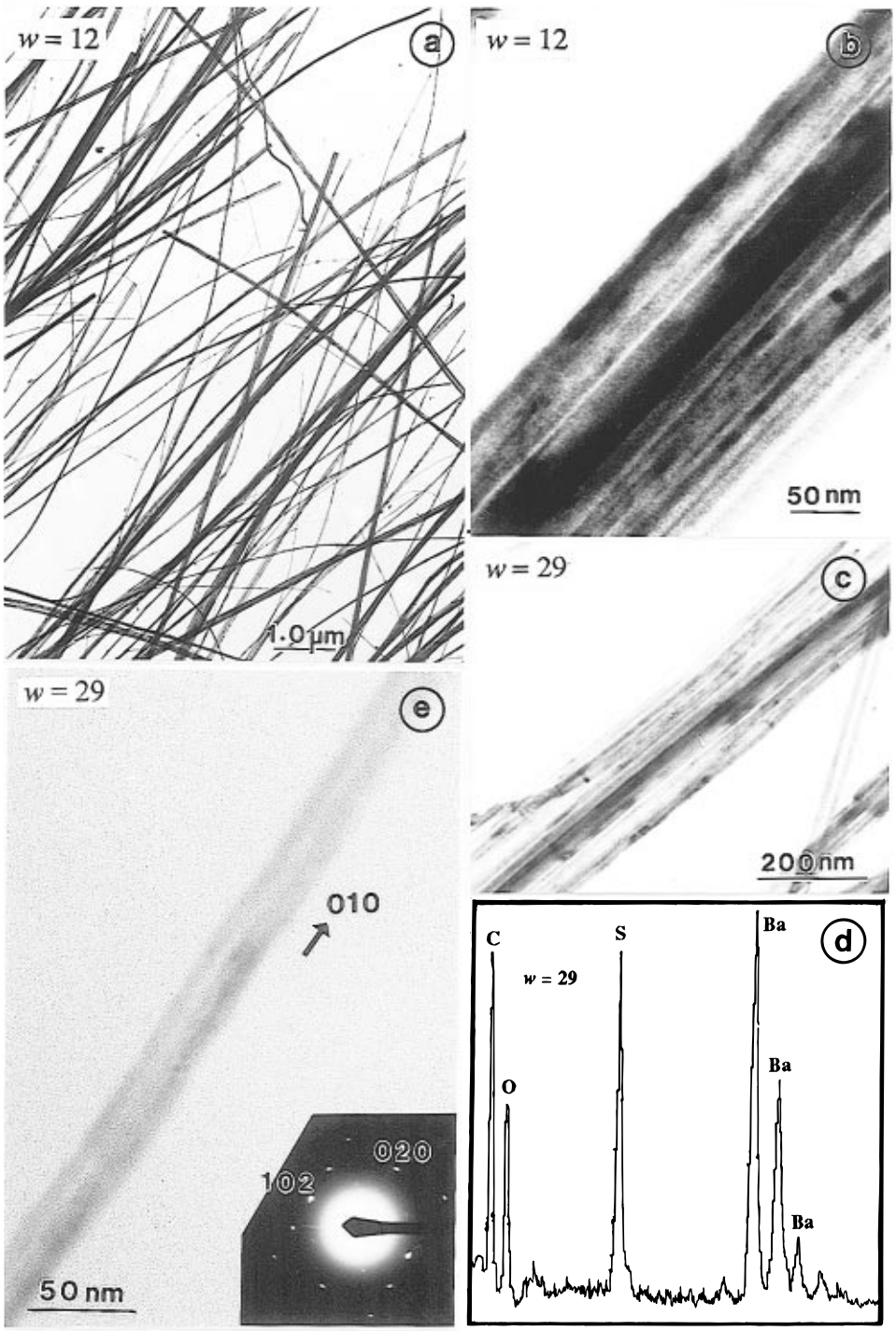

Figure 3. (a) Individual $BaSO_4$ filaments formed within a supersaturated ($S > 500$) $Ba_{0.019}Na_{0.962}AOT$ microemulsion, $w = 12$, [AOT] = 0.1 M. (b and c) High magnification TEM images of individual filaments at $w = 12$ and 29, respectively, showing well-defined thickness fringes running parallel to the morphological long axis. (d) EDXA spectrum recorded from an individual $BaSO_4$ filament. (e) Individual filament and associated electron diffraction pattern (inset). The filament is a single barite crystal viewed along the [20$\bar{1}$] zone. The filament is elongated along the crystallographic [010] axis.

Supersaturated $Ba_{0.019}Na_{0.962}AOT$ microemulsions with a surfactant to oil concentration of 0.1−0.3 M and $w = 10-29$ were usually prepared as for the reverse micelle solutions except that the isooctane solution of $BaAOT_2$ (0.05 mol dm^{-3} oil) was added to dispersions of NaAOT/isooctane/water microemulsions prepared with different amounts of aqueous 0.02 M Na_2SO_4 solution. A second method, in which $BaSO_4$ particles were prepared by rapidly mixing a NaAOT/isooctane/H_2O microemulsion containing 0.01 M $BaCl_2$ solution with a NaAOT microemulsion of equal surfactant concentration (0.272 mol dm^{-3} oil) and w value, but containing 0.01 M Na_2SO_4 solution, was used to prepare supersaturated $Ba_{0.005}Na_{0.990}AOT$ and $Ba_{0.006}Na_{0.988}AOT$ microemulsions ($w = 49$ and 66, respectively). Up to 30 min was required for solubilization of the 0.01 M $BaCl_2$ solution compared with 5 min for preparation of the Na_2SO_4-containing microemulsions. In general, this method was limited by the low concentrations of Ba^{2+} ions that could be incorporated into the microemulsions due to phase separation in the presence of solutions with high ionic strength.

Barium Sulfate Formation in $C_{12}EO_4$ Reverse Micelles and Microemulsions. Barium sulfate particles were prepared by rapidly mixing 5 g of a $C_{12}EO_4$/decane/H_2O reverse micelle solution containing 1.0 or 20 mM $BaCl_2$ solution with an equal weight of $C_{12}EO_4$ reverse micelles of equal surfactant concentration (0.38 mol dm^{-3} oil) and w value (=4), but containing 1.0 or 20 mM Na_2SO_4. This procedure was repeated for $C_{12}EO_4$/decane/H_2O microemulsions with w value of 15. Samples were extracted after 1 week.

Barium Sulfate Formation in DDAB Microemulsions. DDAB/dodecane/H_2O microemulsions containing either $BaCl_2$ or Na_2SO_4 solutions were prepared and mixed as described for the $C_{12}EO_4$ microemulsions. The surfactant concentration was 1.62 mol of DDAB dm^{-3} dodecane, and a w value of 15 was used. Samples were extracted after 1 week.

Calculation of Barium Sulfate Supersaturation. The supersaturation ratio was calculated using the equation

$$S = \{[(\gamma c_{Ba^{2+}})(\gamma c_{SO_4^{2-}})]/[K_{sp}]\}^{0.5}$$

where γ is the divalent ion activity coefficient, c the concentration of nonassociated barium and sulfate ions (mol dm^{-3}), and K_{sp} the solubility product of crystalline barium sulfate (mol^2 dm^{-6}). The activity coefficients were solved using the computer program IONPRODUCT.[41] While the above equation was used to calculate S values for reverse micelles and microemulsions containing neutral ($C_{12}EO_4$) or positively charged (DDAB) surfactants, it is probably invalid for the AOT systems because of strong Ba^{2+} interactions at the anionic headgroups. Thus, supersaturation values calculated for these experiments are likely to be significantly lower than in the real system.

Electron Microscopy. Particles for transmission electron microscopy were collected from micellar dispersions using a glass pipet and deposited onto Formvar-coated, carbon-reinforced, copper electron microscope grids. The samples were air-dried for 2−3 s after which the liquid (now partly a liquid-crystal film) was washed for 10 s by immersing the grid in pure solvent. The grid was then removed and air-dried.

TEM analysis was performed in bright field mode using either a JEOL 1200 EX electron microscope operating at 120 keV or a JEOL 2000 FX high-resolution electron microscope operating at 200 keV. The imaged crystals were characterized by selected area electron diffraction (SAED) and energy-dispersive X-ray analysis (EDXA). The former were indexed with reference to the unit cell of barium sulfate (space group *Pnma*, a, b, c = 8.909, 5.467, and 7.188 Å).

Samples for thin sectioning were removed by pipet, dispersed in isooctane and then acetone, and then polymerized in epoxy resin. Thin sections (60−100 nm) were cut using a glass knife and mounted onto carbon-coated grids for TEM examination. Samples were also analyzed in situ by optical microscopy using a Zeiss Axiphot transmission light microscope in phase contrast mode. X-ray diffraction data were obtained from dry samples using a Philips PW 1710 powder diffractometer.

Results

$BaSO_4$ Synthesis in BaNaAOT Reverse Micelles. $Ba_{0.019}$ $Na_{0.962}$ AOT reverse micelle solutions (w = 5, S > 800) were initially colorless and transparent but over a period of 24 h became blue and translucent due to light scattering. The coloration became more intense after 1 week, but no bulk precipitation was observed.

At low micellar concentration ([AOT] = 0.1 M), small oval-shaped particles, 70−150 nm long and 50−100 nm wide, were observed by electron microscopy (Figures 1a,b). At high magnification, these particles appeared to consist of aggregates of low contrast nanoclusters which were roughly spherical and between 2 and 4 nm in diameter. Elemental analysis (EDXA) showed that the aggregates and nanoparticles consisted of Ba, S, and O (Figure 1c). No electron diffraction patterns were obtained indicating that the barium sulfate phase contained within the nanoparticles was predominantly amorphous.

(41) Shellis, R. P. *CABIOS, IRL Press Limited*; Oxford: England, 1988; Vol. 3, p 373.

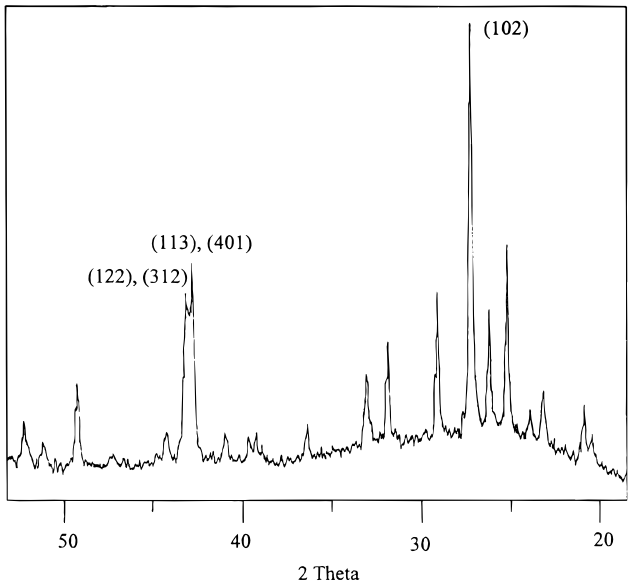

Figure 4. Powder XRD pattern for $BaSO_4$ filaments formed within a $Ba_{0.019}Na_{0.962}$AOT microemulsion, w = 12, [AOT] = 0.1 M.

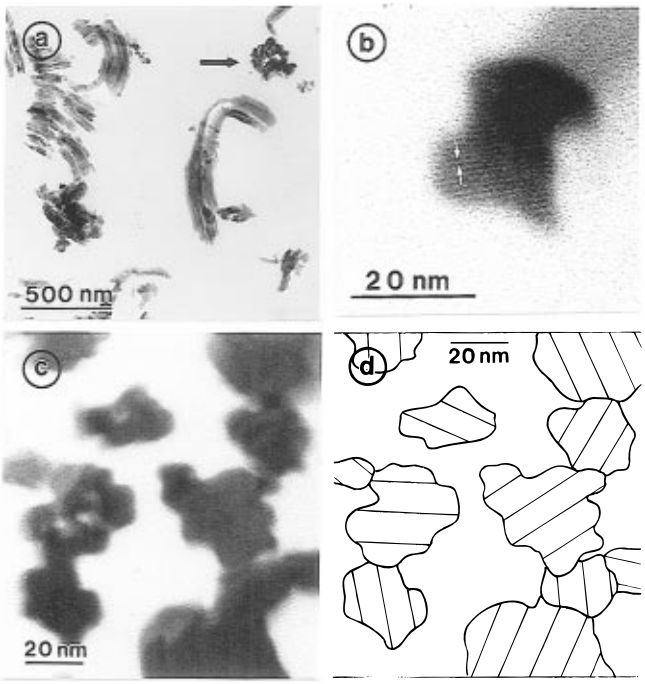

Figure 5. Thin sections of $BaSO_4$ filaments formed from BaNaAOT microemulsions at w = 12, [AOT] = 0.1 M. (a) Low magnification TEM image showing several filaments with internal structure cut in different orientations. A transverse section of a single filament is highlighted (arrow). (b) Lattice image, showing continuous fringes running across a single filament. The fringe spacing is ca. 0.9 nm, corresponding to the (100) planes of barite. (c) High magnification image of a single filament showing porous internal structure and curved edges of the constituent nanofilaments. (d) Sketch highlighting the cross section of the internal filaments shown in (c).

Oval-shaped aggregates comprising amorphous $BaSO_4$ nanoparticles were also observed at a higher surfactant concentration of 1.46 M (Figures 1d,e). The nanoparticles were 2−5 nm in diameter and hence of similar size to those formed in reverse micelles at a lower surfactant concentration. However, the aggregates were much larger, typically 200−250 nm long and 130−150 nm wide. Furthermore, larger agglomerates, con-

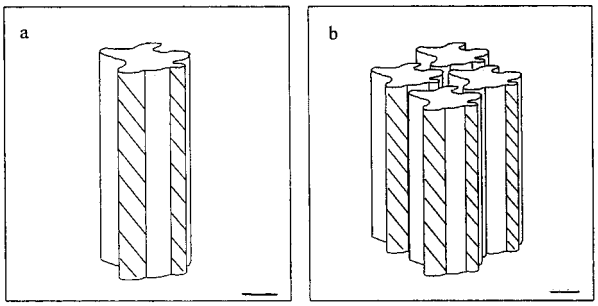

Figure 6. Sketches of (a) single nanofilament of crystalline $BaSO_4$, scale bar = 20 nm, and (b) coherently aligned arrangement of nanofilaments in a composite $BaSO_4$ whisker; scale bar = 20 nm.

taining up to 10 of these aggregates, were often observed.

$BaSO_4$ Synthesis in BaNaAOT Microemulsions. Supersaturated ($S > 500$) $Ba_{0.019}Na_{0.962}AOT$/isooctane/H_2O microemulsion solutions, prepared by mixing $BaAOT_2$ reverse micelles with sulfate-containing NaAOT microemulsions, were initially colorless and transparent but became cloudy over a period of 1 week. White, sometimes gellike, deposits were observed, and these, as well as samples taken from solution, were analyzed by TEM and optical microscopy. Over 95% of the particles from each sample were fibrous. At $w = 10$, the fibers were 2−20 μm long and noncompact in shape, often comprising loosely divergent strands, 50−500 nm in width, which emanated from the ends of the fibers (Figure 2). At $w = 12-29$, single filaments, 1−100 μm long and 20−200 nm wide, were observed (Figure 3a). The filaments had straight edges, uniform widths, and often well-defined flattened ends. A typical aspect ratio was 1000. Like the multiple fibers at $w = 10$, the single filaments often showed electron dense thickness fringes with spacings of 10−20 nm, running parallel to the morphological axis (Figures 3b,c). Barium, S, and O were detected by EDXA (Figure 3d). Electron diffraction analysis of nine individual filaments indicated that they were single crystals of barite. Eight patterns showed that the filaments were elongated along the [010] crystallographic axis (Figure 3e). High-resolution TEM micrographs showed coherent and continuous lattice images traversing the thickness fringes, confirming the single-crystalline nature of the filaments (data not shown). Powder X-ray diffraction patterns of the filaments consisted of narrow peaks with *d* spacings consistent with well-ordered crystalline barite (Figure 4) .

Transverse thin sections of the wider $BaSO_4$ filaments formed from BaNaAOT microemulsions at $w = 12$ showed an internal structure composed of thinner filaments (20−50 nm in width) which had irregular cross-sectional shapes with negative and positive curvature (Figure 5). In some sections, a porous internal structure was observed in localized regions. Continuous and coherent lattice fringes, with *d* spacings consistent with barite, were imaged in the cross-sectioned filaments (Figure 5b). Together, these results and those obtained from unsectioned samples, suggest that the individual filaments are formed either as single whiskers or consist of coherently aligned nanometer-sized filaments of barite single crystals (Figure 6). The composite filaments have pronounced fluted edges

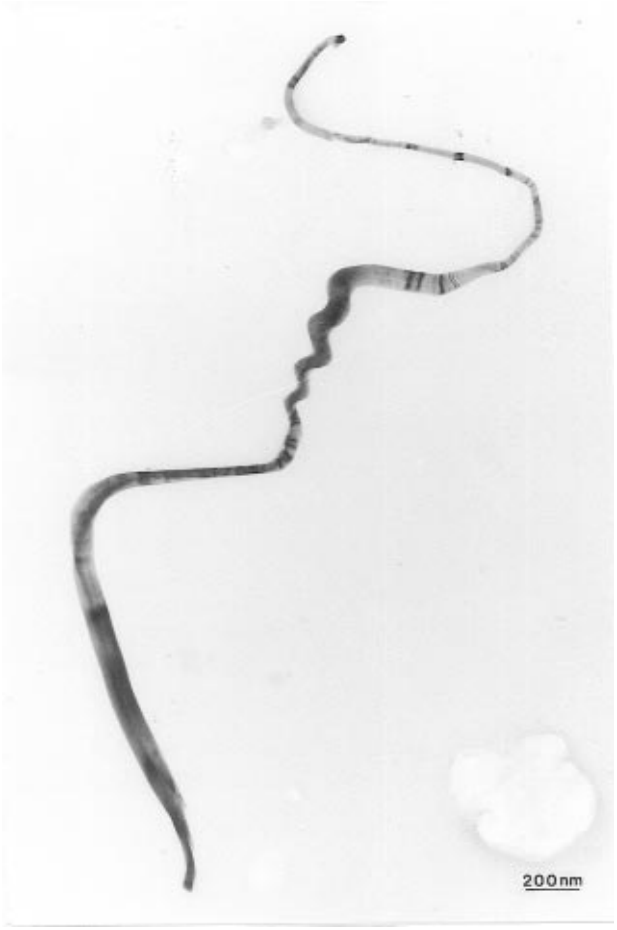

Figure 7. TEM image of a single twisted filament of crystalline $BaSO_4$ formed in supersaturated microemulsions ($w = 66$, [AOT] = 0.27 M) produced by rapidly mixing preformed AOT/isooctane/H_2O microemulsions containing 0.01 M Ba^{2+} or 0.01 M SO_4^{2-} at room temperature.

which give rise to the parallel thickness fringes observed by TEM.

Similar results were obtained by mixing Ba^{2+}-containing microemulsions with sulfate-containing microemulsions at $w = 49$ and 66, and $S > 190$. However, the yield of individual barite filaments was increased under these conditions. The filaments were 2−5 μm long and 50−100 nm wide and often showed diffraction contrast perpendicular to the long axis associated with a twisted and convoluted morphological form (Figure 7).

$BaSO_4$ Synthesis in $C_{12}EO_4$ Reverse Micelles and Microemulsions. Supersaturated $C_{12}EO_4$/decane/H_2O reverse micelles ($w = 4$, $S = 33$ or 270) were optically transparent and stable with respect to phase separation. Inorganic particles were readily observed only at $S = 270$ presumably because of the low yields at $S = 33$. TEM images showed irregular aggregates of spherical or oval-shaped electron dense nanoparticles (5−7 nm in size) after 1 week (Figure 8a,b). EDXA detected Ba, S, and O (data not shown), and powder electron diffraction patterns were consistent with the lattice spacings of barite (Figure 8c), indicating that nanocrystals were formed within the $C_{12}EO_4$ reverse micelles.

Barium sulfate particles were observed after one week in $C_{12}EO_4$ microemulsions ($w = 15$) with supersaturations of $S = 33$ and 270. The solutions remained viscous and stable with respect to phase separation during inorganic crystallization. At $S = 33$, the particles were

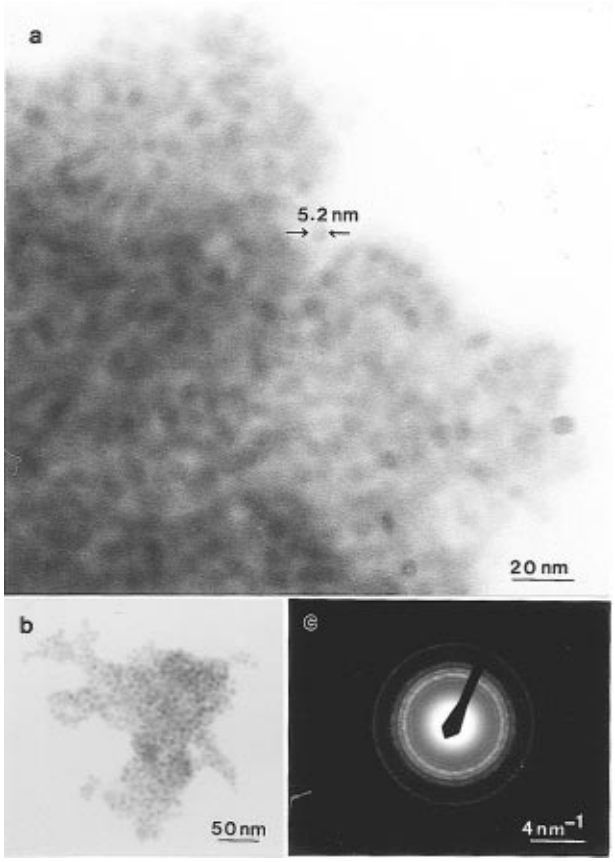

Figure 8. Barium sulfate precipitation in supersaturated $C_{12}EO_4$/decane/H_2O reverse micelles, at $w = 4$, $S = 270$, $[C_{12}EO_4] = 0.2$ M. (a) High magnification TEM image showing aggregated nanocrystals of $BaSO_4$. (b) Low magnification image of the aggregated material. (c) Electron diffraction powder pattern from an aggregate with barite *d* spacings.

tabular in shape, with dimensions of 50−100 nm in width and 100−400 nm in length. The crystals were truncated by smooth prismatic faces and had roughened concave sides depending on the extent of crystal growth (Figure 9a,c,d). Electron diffraction patterns indicated that each particle was a single crystal of barite (Figure 9a,c,d) and that the direction of elongation corresponded to the [100] crystallographic axis. The tabular surface was identified by electron diffraction as the (001) face, the prismatic faces as {210}, and the roughened edges were indexed as {*hk*0}. High-resolution TEM images revealed coherent lattice fringes indicating that the crystals were highly structured. No microfacets were observed on the roughened side faces (Figure 9b).

Increasing the supersaturation to $S = 270$ resulted in smaller crystals of mixed orientation (Figures 9e). These were heterogeneous in size, ranging in length from 10 to 60 nm. Some of the crystals were pseudohexagonal in shape, whereas others were rectangular or rhombic. Powder electron diffraction patterns confirmed the particles as single crystals of barite.

$BaSO_4$ Synthesis in DDAB Microemulsions. Supersaturated DDAB microemulsions ($w = 15$) were optically transparent, viscous, and stable with respect to phase separation. Those prepared at $S = 33$ and sampled after 1 week, contained rhombic prisms of barite (Figures 10a,b). In general, the prisms were 200 nm long, 150 nm wide, and 60 nm thick and were therefore of a size similar to the tablets grown at $S = 33$ in $C_{12}EO_4$ microemulsions but with a different crystal morphology. Electron diffraction analysis of individual crystals gave single-crystal patterns and identified the tabular and prismatic surfaces as the (001) and {210} faces of barite, respectively.

Discussion

The results indicate that the precipitation of barium sulfate in supersaturated reverse micelles and microemulsions can be markedly influenced by the nature of the surfactant and supramolecular architecture of the self-assembled aggregates. The most surprising observation concerns the formation of highly elongated nanofilaments of barite single crystals in AOT microemulsions—a result that was completely unexpected. This phenomenon appears to be restricted to the sulfonate headgroups of AOT under the experimental conditions investigated, as similar reactions in $C_{12}EO_4$ and DDAB microemulsions produced regular particles with geometric shapes. However, we propose a general mechanism for the formation of the filaments, rather than one based on specific molecular interactions, for the following reasons. First, the formation of the barite filaments was essentially independent of the method of preparation, either by addition of $BaAOT_2$ reverse micelles to sulfate-containing NaAOT microemulsions, or by mixing equal volumes of barium-containing and sulfate-containing NaAOT microemulsions over a range of *w* values. Second, experiments using AOT microemulsions were repeated with Ba^{2+}/CO_3^{2-} solutions, and highly elongated, crystallographically oriented fibers of witherite ($BaCO_3$) were formed in high yield.[42] Third, filamentous $BaSO_4$ crystals have been produced by crystallization in aqueous solutions containing relatively high concentrations of polycarboxylates such as polyacrylates[42,43] or polymaleates.[44] And fourth, crystallization of $BaSO_4$ from aqueous solutions of NaAOT at $S = 22$ resulted in a general roughening of the crystal surfaces, indicating a nonspecific mechanism for surface adsorption of the surfactant.[42]

In the absence of unbound water, addition of anhydrous $BaAOT_2$/isooctane solutions to sulfate-containing NaAOT reverse micelles with $w = 5$, produces surfactant/$BaSO_4$ nanoparticles which are amorphous in structure and commensurate in size with the polar-core diameter ($d \approx 2$ nm at $w = 5$) reported for NaAOT reverse micelles.[45] The noncrystalline nature of these particles suggests that nucleation proceeds rapidly, presumably within the "dry" $BaAOT_2$ aggregates. Because the theoretical supersaturation attainable within the confined volumes on mixing is very high (>800), nucleation of $BaSO_4$ clusters is expected to occur at the onset of aqueous phase transfer from the sulfate-containing reverse micelles. This implies that the interacting micelles would be fused irreversibly by mutual association with $BaSO_4$ nuclei formed at the collision interface. In addition, further fusion processes with other sulfate-containing micelles would result in long-range aggregation as shown in Figure 1a. The exchange rates for reverse micelles are known to be very slow due to the high microviscosity of the condensed

(42) Hopwood, J. D. *Ph.D. Thesis*, University of Bath, 1996.
(43) Brase, I. E. U.S. Patent 4898677, 1990.
(44) Benton, W. B.; Collins, I. R.; Parkinson, G. M.; Rodger, S. A. *Faraday Discuss.* **1993**, *95*, 281.
(45) Robinson, B. H. *Chem. Britain* **1990**. *26*, 333.

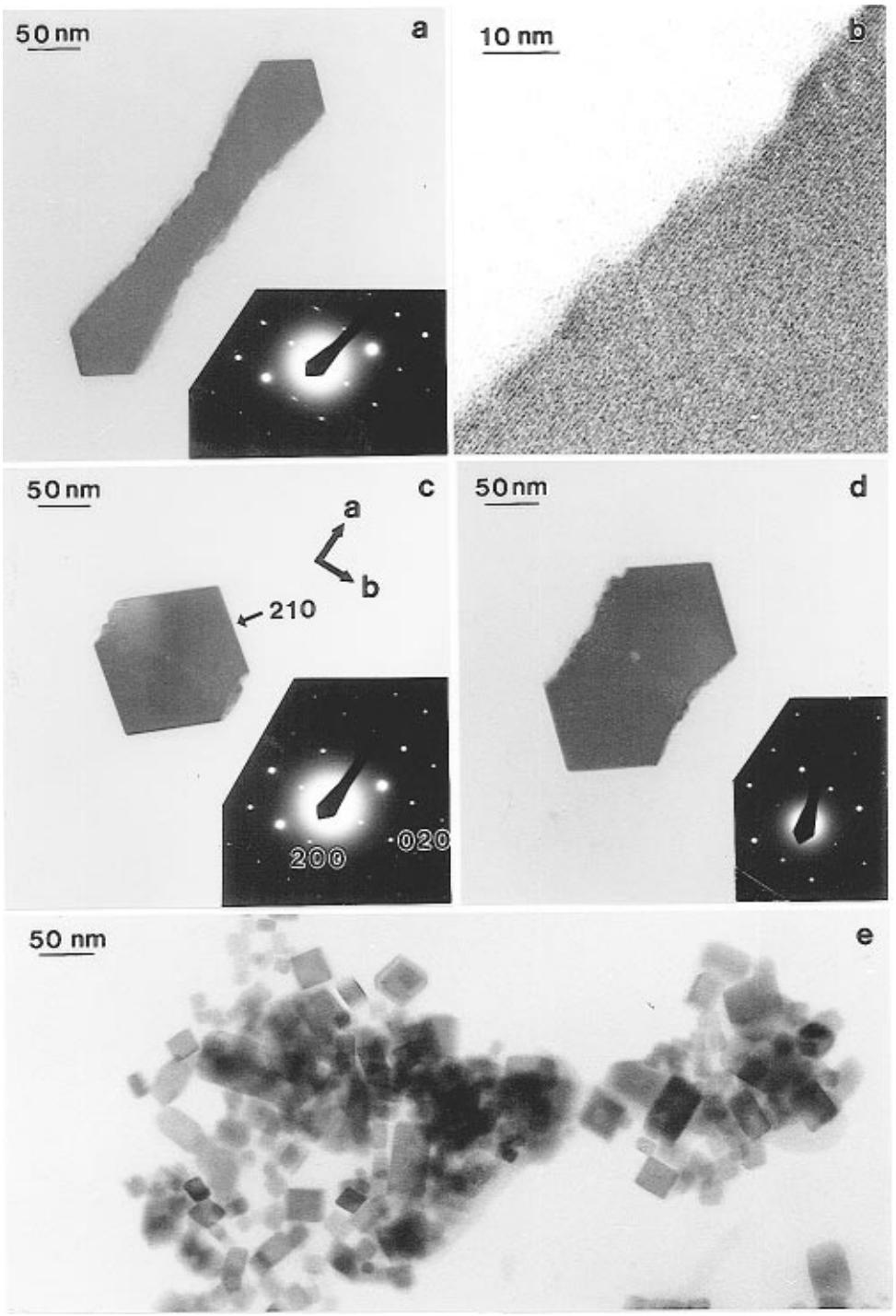

Figure 9. (a−d) Barium sulfate formation in supersaturated $C_{12}EO_4$/decane/H_2O microemulsions, at $w = 15$, $S = 33$, $[C_{12}EO_4] = 0.38$ M. (a, c, and d) TEM images of individual crystals showing well-defined {210} end faces and concave side faces with variable levels of expression. Insets show corresponding electron diffraction patterns. In each case the pattern corresponds to the [001] zone of barite and the crystals are elongated along the [100] direction (*a* axis) of the unit cell. See inset in (c) for indexing of diffraction reflections. (b) High-resolution micrograph of roughened side face showing coherent barite lattice images. (d) barite crystals grown in supersaturated $C_{12}EO_4$/decane/H_2O microemulsions, at $w = 15$, $S = 270$, $[C_{12}EO_4] = 0.38$ M.

aggregates,[46] so that although nucleation of individual clusters would be very fast, the aggregation process would be relatively slow. Furthermore, strong binding interactions between the sulfonate headgroups and inorganic phase could be responsible for the apparent stability of the disordered $BaSO_4$/surfactant complex. By comparison, interactions between Ba^{2+} cations and the polyether headgroups of $C_{12}EO_4$ reverse micelles are less strong, with the consequence that the pathway to barite nucleation is sterically and kinetically unhindered within the polar core.

The dramatic change in behavior accompanying an increase in the *w* value from 5 to 10 for the AOT system, strongly suggests that the presence of bulk, exchangeable water molecules in the microemulsions is of key importance for filament formation. The dimensions of the barite filaments are clearly incommensurate with those of individual AOT microemulsions, suggesting that aggregation and coalescence of individual droplets are important aspects of the growth mechanism. The

(46) Terpko, A. T.; et al. *J. Colloid Interface Sci.* **1981**, *84*, 202.

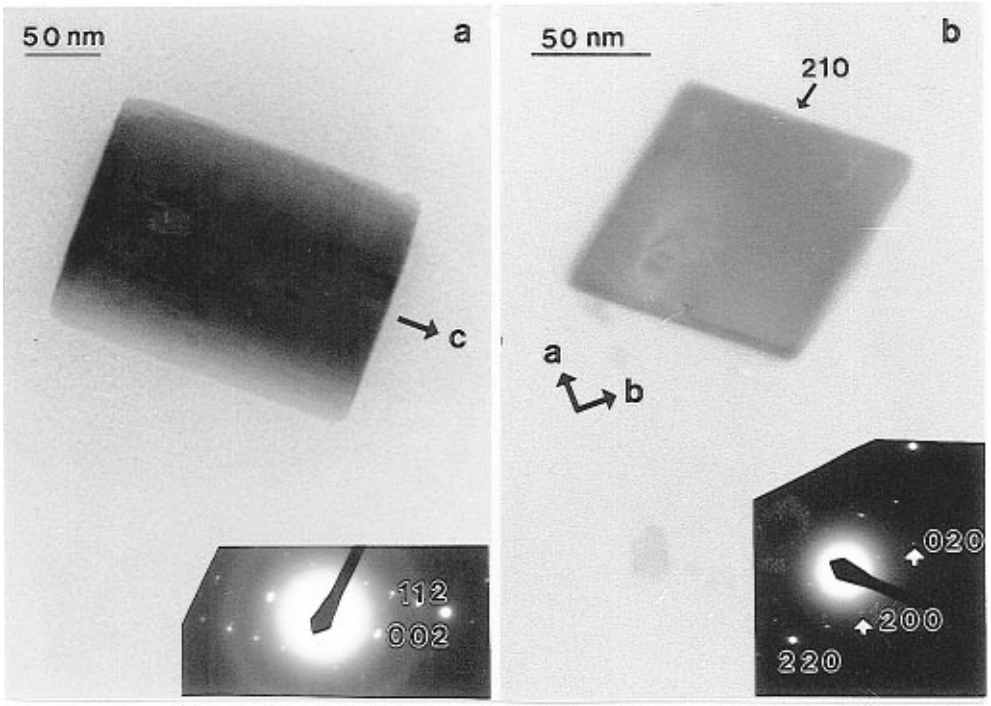

Figure 10. Barium sulfate synthesis in supersaturated DDAB/dodecane/H_2O microemulsions, at $w = 15$, $S = 33$, [DDAB] = 1.62 M. (a) Prismatic barite crystal elongated along the [001] direction (*c* axis); inset shows corresponding electron diffraction pattern. (b) Similar prismatic crystal but viewed along the [001] axis with {210} faces.

extremely high aspect ratio suggests that the fusion processes are irreversible, unidirectional, and possibly autocatalytic; in the initial stages of formation this implies that nanofilaments, perhaps one microemulsion droplet wide (4 nm), are propagated through the medium. If, as suggested above, inorganic nucleation and irreversible micellar fusion are coincident due to the former being significantly faster than the rate of dissociation, then a similar fusion event between two spherical microemulsion droplets would result in a short cylindrical droplet. Such a droplet would comprise a centrally located amorphous $BaSO_4$/surfactant complex with water-enriched domains at the ends of the shaped aggregate (Figure 11). Dynamic exchange with other microemulsion droplets would then be significantly faster at the ends of the fusion pair than in the central region containing the nucleated cluster because surfactant molecules in the vicinity of the laterally displaced water molecules can dissociate into the oil phase without dehydrating the adjacent headgroups.[47] In contrast, the surfactant molecules associated with the centralized $BaSO_4$ complex would be immobile.

In this model, the spatial localization of unbound water molecules provides the necessary anisotropy for the generation of the nanofilamentous inorganic morphology. Growth of the inorganic phase is essentially restricted to the ends of the filaments which are capped with microemulsion hemispheres undergoing slow exchange and coalescence. By contrast, the filament sides are blocked by a monolayer of strongly bound AOT molecules. However, microemulsion droplets must interact with this surface if the filaments are to attain the observed width of approximately 20−50 nm. One possibility is that individual droplets slowly self-assemble and fuse along the side faces of the nanofilament

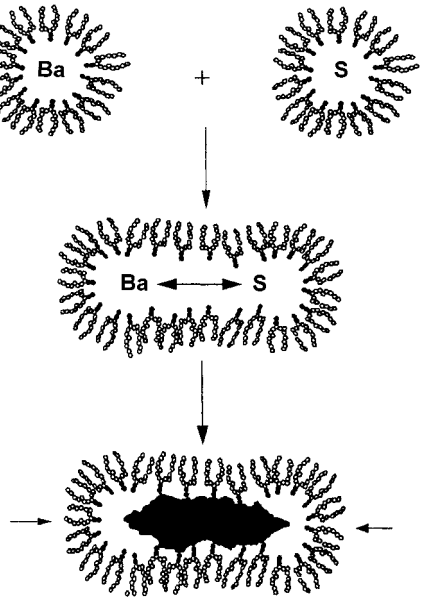

Figure 11. Proposed mechanism for the formation of barite nanofilaments in AOT microemulsions. Fusion results in rapid nucleation of an amorphous $BaSO_4$/surfactant phase that induces anisotropy into the collision pair due to differences in the exchangeability between bound and unbound surfactant molecules. The latter remain hydrated and are laterally displaced such that further exchange and $BaSO_4$ deposition are restricted along a unidirectional axis (arrows). $S = SO_4^{2-}$.

by interdigitation of the organic chains. This would explain the formation of the coherently aligned nanofilaments and the surface corrugations observed in the electron micrographs of the composite filaments.

Finally, our model implies a strong association between the $BaSO_4$ clusters and AOT molecules throughout the development of the filaments. This is less likely to occur if the inorganic phase is ordered because the organized reaction field generated by the surfactant

(47) Clark, C.; Fletcher, D. I.; Xilin,Y. *Langmuir* **1990**. *6*, 1301.

assemblies can be offset by the lattice and surface energies of the growing crystal. This appears to be the case for both $C_{12}EO_4$ and DDAB microemulsions, which have negligible influence on the size and shape of the barite crystals. Thus, we propose that the single-crystalline nature of the barite filaments produced in AOT microemulsions, as well as their co-aligned filamentous domain structure, originate from the phase transformation of an amorphous $BaSO_4$ precursor with the same morphology. The fact that the filaments are crystallographically aligned along the [010] axis suggests that epitaxial nucleation of barite at the surfactant interface might be an important aspect of this phase transformation mechanism.

Acknowledgment. We thank Dr. M. Lees for helpful discussions and FMC Corp. for support of a postgraduate studentship to J.D.H.

CM970113Q